GEOPHYSICS, VOL. 81, NO. 5 (SEPTEMBER-OCTOBER 2016); P. F49–F57, 7 FIGS.
10.1190/GEO2015-0320.1

Inversion of controlled-source electromagnetic reflection responses

Jürg Hunziker[1], Jan Thorbecke[2], Joeri Brackenhoff[2], and Evert Slob[2]

ABSTRACT

Marine controlled-source electromagnetic reflection responses can be retrieved by interferometry. These reflection responses are free of effects related to the water layer and the air above it and do not suffer from uncertainties related to the source position and orientation. Interferometry is a data-driven process requiring proper sampling of the electromagnetic field as well as knowledge of the material parameters at the receiver level, i.e., the sediment just below the receivers. We have inverted synthetic data sets using the reflection responses or the original electromagnetic fields with the goal of extracting the conductivity model of the subsurface. For the inversion, a genetic algorithm and a nonlinear conjugate-gradient algorithm were used. Our results show that an inversion of the reflection responses produces worse estimates of the vertical conductivity but superior estimates of the horizontal conductivity (especially for the reservoir) with respect to the original electromagnetic fields.

INTRODUCTION

For this study, we consider frequency-domain marine controlled-source electromagnetics (CSEM). In marine CSEM, a boat tows a source that emits an electric signal. The resulting earth response is recorded with electromagnetic receivers located at the ocean bottom. In frequency-domain CSEM, the source signal is, in most cases, a square wave with a base frequency and several harmonics. However, only the peak frequency and sometimes also the higher harmonics are used for the interpretation. In our numerical examples, we consider only the peak frequency of 0.5 Hz. For an overview of this method, we recommend the paper of Constable (2010).

Because the electromagnetic signal at those frequencies is a diffusive field, interpretation is not straightforward. Usually, an inversion of the data is carried out. This process searches for the subsurface conductivity distribution that best explains the measured data. This search is done by minimizing in some way the difference between the measured and the forward modeled data based on the latest guess of the subsurface conductivity distribution. Because this is a major topic of CSEM research, a wide variety of papers have been published on inversion (Christensen and Dodds, 2007; Plessix and Mulder, 2008; Key, 2009; Brown et al., 2012; Ray et al., 2013; Sasaki, 2013; Wiik et al., 2013; Grayver et al., 2014).

In this paper, we discuss the inversion of reflection responses in contrast to the inversion of the full electromagnetic fields. The reflection responses used here, sometimes also called the scattered Green's function of the subsurface, are unitless and free of events related to the water layer and the air above it. This means that the direct field is suppressed. The same is true for the airwave, the signal that diffuses upward from the source and is refracted in the air where it propagates as an almost undamped wave with the speed of light. In standard CSEM data, these two events cover the subsurface signal at short offsets (direct field) and in shallow marine situations at large offsets (airwave). By suppressing these events, the data more strongly depend on the subsurface than on the water and air above it.

The reflection responses consist of signals traveling between receivers (turning a receiver into a virtual source) and removing the dependence on the actual source. Because the source is towed behind a boat in marine CSEM measurements, the position and orientation of the source can be influenced by factors that lie outside the control of the source operator, such as, for example, water currents. Source position and orientation uncertainty causes errors in the forward-modeling step of the inversion. Because the receivers are usually stationary on the ocean bottom (Constable, 2010), this issue can be mitigated by using the reflection responses instead of the original electromagnetic fields in the inversion.

Peer-reviewed code related to this article can be found at http://software.seg.org/2016/0005.
Manuscript received by the Editor 16 June 2015; revised manuscript received 28 January 2016; published online 18 July 2016.
[1]Formerly Delft University of Technology, Department of Geotechnology, Delft, The Netherlands; presently Université de Lausanne, Institut des Sciences de la Terre, Lausanne, Switzerland. E-mail: jurg.hunziker@unil.ch.
[2]Delft University of Technology, Department of Geotechnology, Delft, The Netherlands. E-mail: j.w.thorbecke@tudelft.nl; j.a.brackenhoff@student.tudelft.nl; e.c.slob@tudelft.nl.

The reflection responses can be retrieved from CSEM data by applying interferometry. In seismics, interferometry is often applied as a crosscorrelation process (Bakulin and Calvert, 2006; Draganov et al., 2006; Wapenaar and Fokkema, 2006). This method assumes the medium to be lossless, which is not true for diffusive fields in CSEM. Therefore, we apply interferometry by multidimensional deconvolution (MDD), which is valid for media with losses (Wapenaar et al., 2008). Because interferometry uses the information that is stored in the data to redatum the source, suppress the direct field, and replace the overburden with a homogeneous half-space, no information about the water layer or the source position and orientation is required. However, interferometry by MDD works with upward and downward decaying fields. This decomposition (see the appendix of Slob, 2009) also separates the electromagnetic field into the transverse magnetic (TM) mode and the transverse electric (TE) mode at the receiver level. To perform this decomposition, the material parameters at the receiver level need to be known. Because the receivers are located at the ocean bottom, i.e., at the interface between the water and the sediment, either the conductivity of the water or that of the sediment can be used. Correspondingly, the receivers are considered to be located just above the interface in the water or just below the interface in the sediment. To suppress any effect of the water on the data, it is crucial to use the conductivity of the sediment for this decomposition. Furthermore, to access the information stored in the data, the electromagnetic field needs to be sampled on a grid. The sampling is required to be dense enough and without any gaps. The method also assumes that the ocean bottom is flat. Hunziker et al. (2012) show that the data can be sampled more sparsely if the synthetic-aperture-source concept (Fan et al., 2010) is used, and that the method also works with noisy data, as is the case under realistic conditions.

Interferometry by MDD basically consists of two steps (Hunziker et al., 2012, 2013). In the first step, the diffusive fields are decomposed in upward and downward decaying TM- and TE-modes. The second step consists of the actual MDD. Thereby, any upward decaying component (either TM- or TE-mode) is deconvolved over space and time with any downward decaying component to retrieve the reflection response of the subsurface. If an upward decaying TM-mode component is deconvolved with a downward decaying TM-mode component, the TM-mode reflection response is retrieved. Correspondingly, the TE-mode reflection response can be retrieved. Reflection responses, containing conversions from one mode to the other, are also possible by deconvolving the components accordingly. However, in a layered medium, as it is used in this study, no conversions between the TM- and the TE-mode happen (see, e.g., the appendix of Hunziker et al., 2013). Thus, we consider here only pure TM- and TE-mode reflection responses.

The above-outlined properties of reflection responses motivated us to investigate the performance of inversions of the CSEM reflection response compared with inversions of the corresponding original CSEM data. For this study, we apply two different inversion algorithms to the two types of data sets. First, we use a genetic algorithm, which is a global optimization routine, to find the conductivity of a layered medium that features vertical transverse isotropic (VTI) anisotropy. Second, we use a nonlinear conjugate-gradient algorithm, which is a local optimization routine, to invert for a layered isotropic medium. The second algorithm is included in this paper because it is not straightforwardly implemented, as explained below. In the next section, we explain the two algorithms. Then, the results for the genetic algorithm are presented followed by those for the conjugate-gradient algorithm. At the end of the paper, a short discussion of the results is presented and our conclusions are drawn.

METHODS

Genetic algorithm

This algorithm mimics evolution theory to find the conductivity distribution of the subsurface that explains the data best. The algorithm starts with a set of random guesses in which each guess is a complete subsurface model. In this algorithm, belonging to the group of stochastic algorithms, some events occur in a random fashion as outlined below. Therefore, each run of this algorithm with the same parameter values ends at slightly different solutions. In the framework of evolution theory, we consider each guess an independent individual of the population including all guesses. The genome of an individual is a string of characters that encode the guess. For each individual with the conductivities m, the misfit function F is computed:

$$F=\sum_{i=1}^{N}\frac{[\Re(d_i^{\mathrm{obs}})-\Re(d_i^{\mathrm{mod}}(m))]^2+[\Im(d_i^{\mathrm{obs}})-\Im(d_i^{\mathrm{mod}}(m))]^2}{[\Re(d_i^{\mathrm{obs}})]^2+[\Im(d_i^{\mathrm{obs}})]^2+\varepsilon}, \tag{1}$$

where d_i^{obs} is the ith element of the observed data set and $d_i^{\mathrm{mod}}(m)$ is the ith element of the forward modeled data set. Here, $\Re$ and $\Im$ designate the real and the imaginary parts, respectively. Equation 1 is a locally normalized least-squares misfit function. We chose to normalize the misfit function to make the misfit of the different components comparable. In addition, the local normalization ensures that all data points have a similar weight independent of the field's amplitude at that location. The normalization is stabilized with $\varepsilon = 10^{-20}$. With a dipole strength of 1 Am, the stabilization is below the typical noise floor for marine CSEM data given by Constable (2010). For a real or a synthetic data set with noise, no stabilization would be required because the data would never be zero. For forward modeling, we use our publicly available modeling code (Hunziker et al., 2015). A smaller misfit F means that the individual is fitter than another individual with a larger misfit F. As in evolution theory, the fitter the individual, the larger the chances that this guess is able to transmit its properties to the next generation. Note also that individuals with a high misfit are able to pass on their properties to an individual of the next generation, but its chances to do so are smaller.

If an individual is selected for the next generation, there is a certain chance that it undergoes the process of crossover. During this process, two different individuals are cut at the same random location and their tails are interchanged. In this way, two good guesses are recombined. In addition, it is possible that a mutation occurs. In that case, one digit that encodes the guess is exchanged with a random number. This alters one parameter of the guess randomly, and thus it allows the process to jump out of a local minimum.

Our algorithm also contains the processes of eliting and migration. Eliting means that the properties of the best guesses are given to the next generation unaltered to ensure that a good guess is not lost. Similar to mutation, migration also allows the process to jump out of a local minimum by introducing some new, randomly generated individuals to the population. Goldberg (1989) gives a good

introduction to genetic algorithms. Sen and Stoffa (1995) discuss, among other global optimization routines, genetic algorithms specifically for geophysical problems.

For this study, conductivity values are allowed to range between 10^{-4} and 10 S/m, and a constant population size is used. The latter implies that each run of the algorithm starts with a fixed amount of random guesses, which are evolved during the runtime of the algorithm. For each of these guesses, the forward problem needs to be solved at each iteration. In our implementation of the algorithm, this happens in parallel. Ideally, the population size is a multiple of the number of cores to be used, which is 28 in our case. The smallest multiple of 28 for which the algorithm converged to a stable solution within 100 iterations in most of the runs, turned out to be 560. For the same experiment, we run the program 15 times with a different random starting population consisting of 560 individuals. More runs are always better because that results in more solutions, but more runs cost computational time. We decided to use 15 runs. Judging from convergence history, it seemed likely that in that case at least one run per experiment converged to the global minimum. From the resulting 8400 solutions (15 runs times 560 individuals), we use the best 10% for the analysis.

Conjugate-gradient algorithm

The second algorithm is a nonlinear conjugate-gradient algorithm. In contrast to the genetic algorithm, which belongs to the group of stochastic algorithms, this algorithm is a deterministic algorithm. Thus, no random component is involved. This algorithm begins with one user-specified starting model and it will always end up with the same solution if the same starting model is provided and the same parameter values are supplied.

We use the same analytical code to compute the forward model as for the genetic algorithm. For this inversion algorithm, not only the forward problem but also the gradient of the forward problem needs to be computed. This is done analytically by using a modified version of the before-mentioned forward-modeling code (Hunziker et al., 2015). As developing such a code with analytical gradients is rather time-consuming, we include the complete conjugate-gradient inversion scheme implemented in C and Fortran in this paper as an open-source package. The next paragraphs do not only describe the algorithm but also the code.

Note that a numerical forward simulation of the reflection response would allow lateral variations in the model, but requires the use of a decomposition operator in the frequency-wavenumber domain in the course of the forward-modeling step. A numerical scheme such as, for example, finite-difference averages the electromagnetic field over a cell. Our experience has shown that this averaging introduces a systematic error that disrupts the application of the decomposition operator unless the cells are very small. For a successful application to a 3D data set, the grid needs to be extremely dense. Therefore, we use this analytical formulation.

The misfit function M is similar to the one used in the previous algorithm:

$$M = \sum_{i=1}^{N} w_i^2 \{[\Re(d_i^{\text{obs}}) - \Re(d_i^{\text{mod}}(m))]^2 + [\Im(d_i^{\text{obs}}) - \Im(d_i^{\text{mod}}(m))]^2\}, \quad (2)$$

where w is a weighting function that allows to give a different weight to data at different offsets from the source. This compensates the absence of the local normalization in the misfit function of the genetic algorithm. We omitted this normalization to make sure that the analytical computation of the gradient of the misfit function with respect to the material parameters is as simple as possible. This misfit function is implemented in the code in the C-function compmisfit contained in the file iemmod.c.

Our implementation of this nonlinear conjugate-gradient algorithm follows the paper of Shewchuk (1994). The file iemmod.c is the main file containing the basic structure of the inversion algorithm as well as the input-output operations. After the initialization, the forward model and the gradient of the starting model are computed. This is done by calling the C-function emmod stored in the file emmod.c. This function does two things. First, it is checked if the medium is a homogeneous full space. Second, the layer in which the source and the receivers are located are determined. Then, the function kxwmod in the file kxwmod.c is called. Depending on which component needs to be modeled, a different part of this function separated by an if statement is executed. This function is very similar to the corresponding function used in the electromagnetic forward-modeling package mentioned earlier (Hunziker et al., 2015) with the exception that the so-called Fortran routines not only compute the electromagnetic fields but also the gradient of them. Variables starting with the letter d represent variables related to derivatives, and thus related to the computation of the gradient. After the reflection response or the electromagnetic field is computed in the wavenumber domain, the space-domain representation is computed using a Hankel transformation. For an efficient calculation, this Hankel transformation is only carried out for a selective amount of points in the space domain. This Hankel transformation is located in a while loop, which allows to adaptively compute the transformation for more points wherever precision requires it. The response in the space domain is obtained by an interpolation over the transformed points. Because all this is only done for one quadrant of the data set, the remaining quadrants need to be filled in by copying the first quadrant using the corresponding symmetry. Subsequently, the computed field and its gradient are given back to the main program iemmod.

The gradient gives the direction of the update, but it does not specify the size of the step that needs to be taken in this direction. This step length is computed at this point and stored in the variable alpha. The step length can either be determined by fitting a parabola to three points of the misfit function or by a line search. The former requires only two additional evaluations of the forward problem, whereas the latter may require many more. Because the parabola fitting has a relatively high chance of not finding an appropriate step length, the algorithm switches automatically to the line search if that is the case (i.e., if the misfit of the new solution is larger than the misfit of the previous solution). After the step length is determined, the model is updated and the forward problem is solved and the gradient computed for the current model. These steps are repeated until the stopping criteria are fulfilled or the maximum amount of iterations is reached. At every iteration, the latest model is written to the hard drive.

A performance profile of the code indicated that 95% of the compute time is spent in the Hankel transformation back to the space-frequency domain. Therefore, fast Bessel functions could help to improve the performance.

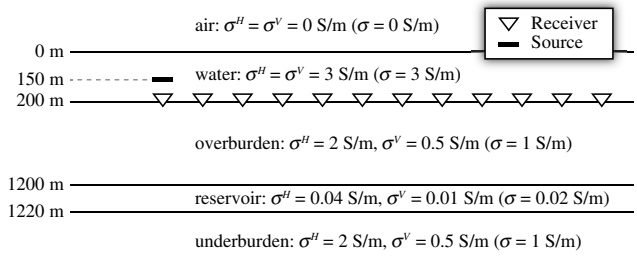

Figure 1. Subsurface model with details about the various layers: Conductivities σ^H and σ^V refer to the VTI medium used for the experiments with the genetic algorithm and conductivities σ given in brackets and without a superscript refer to the isotropic medium used for the experiments with the conjugate-gradient algorithm. Not to scale.

RESULTS

For the experiments discussed here, we created synthetic data based on the model shown in Figure 1. The VTI medium defined by horizontal conductivities σ^H and vertical conductivities σ^V is used for the experiments with the genetic algorithm, whereas the isotropic medium defined by the conductivities σ given in brackets is used for the experiments with the conjugate-gradient algorithm.

The data are computed on a dense grid of receivers at the ocean bottom consisting of 512 times 512 stations separated by 80 m. We have chosen such a dense grid to avoid artifacts in the inversion due to sparse sampling. The source is located at the center and 50 m above this grid. The data are shown as contour plots in Figure 2. Note the radial symmetry and the unitlessness of the reflection responses.

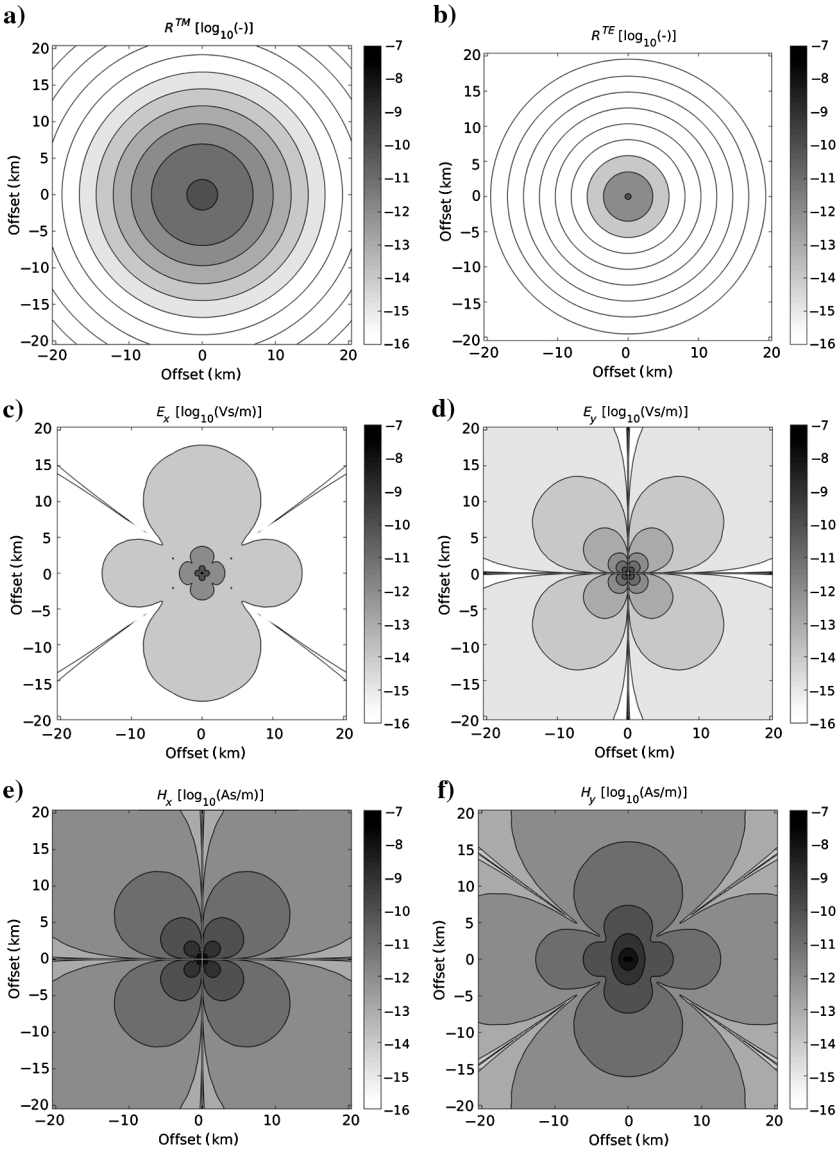

Figure 2. The data sets that are fed to the inversion algorithms: (a) the TM-mode reflection response, (b) the TE-mode reflection response, (c) the inline oriented electric field, (d) the crossline oriented electric field, (e) the inline oriented magnetic field, and (f) the crossline oriented magnetic field. The horizontal axis is thereby parallel to the inline direction and the vertical axis to the crossline direction.

Genetic algorithm

With the genetic algorithm, we estimate four parameters: These are the vertical and horizontal conductivities of the overburden and reservoir layers, respectively. This is of course a small and simple inversion problem. If something does not work on such a simple model, it will also not work in a more complex situation. Naturally, the reverse is not true. Thus, if the inversion of the reflection response does give good results on our simple model, it does not necessarily work on a complex model either. However, this paper is a first tryout of inverting reflection responses with the goal of excluding the approaches that do not work and determine the parameters that cannot be resolved. In this sense, we are convinced that the conclusions drawn from these experiments are also valid for more complicated experiments. Furthermore, we believe that such simple experiments are more instructive than complex experiments because it is much easier to trace what is happening. In a complex experiment, a whole variety of effects are present, making it difficult to figure out what is precisely happening during the processes under investigation.

Note that we estimate the overburden conductivity in this inversion, but that we actually require the conductivity just below the receivers, which is part of the overburden, to retrieve the reflection response by interferometry to begin with. However, this does not influence the inversion process. In theory, the conductivity at the receiver level that we need to know could be an infinitesimally small layer. Thus, the conductivity of the complete overburden is still unknown and still needs to be estimated. It is also important to realize that the reflection at the ocean bottom, which contains information about the overburden layer, is absent in the reflection response, making it more difficult to estimate the overburden conductivity using the reflection response. Also note that the reflection responses used for the inversion are modeled and not retrieved through the interfer-

ometry process. In this way, they are free of artifacts. Again, this is in line with the philosophy outlined in the previous paragraph. If something does not work with the perfect data set, it will certainly also not work if artifacts are present.

Before discussing the actual inversion results, we look at the convergence history of separate inversions of the TM- and the TE-mode reflection responses. Figure 3 shows the misfit of the best solution of each generation for each of the 15 runs. The misfit of the TM-mode inversion decreases six to nine orders of magnitude, and the misfit of the TE-mode inversion decreases four to 15 orders of magnitude. The fact that for the TE-mode many runs decrease over more orders of magnitude than for the TM-mode suggests that the TE-mode inversion was able to find a model that explains the data better than the TM-mode inversion could.

We can also see from Figure 3 that all runs reach a stable misfit, which no longer decreases, before the program ended. This means that the algorithm has converged to a local or a global minimum. Note that each run gives 560 solutions because 560 individuals were evolved in each run. From these 15 times 560 solutions, only the 10% which have the smallest misfit are selected for the analysis. This reduces the chance that solutions that ended in a local minimum are included in the final interpretation.

The final results for the inversions with the genetic algorithm are a group of 840 ($15 \times 560 \times 0.1$) solutions per experiment. They are presented in Figure 4 in the form of boxplots. Each parameter estimate of each experiment is represented by one boxplot consisting of several elements. The circle with the black dot represents the median and the box defines the first and the third quartile of all considered solutions. The antennas outline the range that includes all solutions that are less than 1.5 times the interquartile range away from the box (Tukey, 1977).

Using the TM-mode reflection response, all conductivities are estimated with an acceptable resolution (relatively narrow boxplot) except the horizontal conductivity of the reservoir. However, the true solution is not covered by the extension of the boxplots, making it a wrong estimate. Things are different for the inversion using the TE-mode reflection response. This inversion is unable to make an estimate of acceptable resolution for the vertical conductivity, but gives a very good estimate of the horizontal conductivity (the boxplot is so narrow that it collapsed to a line). This is in line with the observation of, for example, Ramananjaona et al. (2011), who state that the TE-mode is primarily sensitive to the horizontal conductivity.

A joint inversion of the two reflection responses allows us to find the vertical conductivity of the overburden with high resolution, although none of the individual components was able to do so. The estimate of the horizontal conductivity of the overburden is much better than for the TM-mode alone, but worse than for the TE-mode alone. The joint inversion also improves the estimate of the vertical conductivity of the reservoir. The correct value is now included in the spread of the boxplot, which was not the case for the inversion of the TM-mode reflection response, and the resolution of the estimate has been increased compared with the inversion of the TE-mode reflection response. However, the estimate of the horizontal conductivity of the reservoir is much worse than for the inversion of the TE-mode reflection response alone. Thus, although the joint inversion brings an improvement to the estimates of the vertical conductivity, it deteriorates the estimates of the horizontal conductivity. By giving more weight to the TE-mode reflection response, a slight improvement of this result might be possible.

As a comparison, we also run the genetic inversion algorithm for an inversion of full electromagnetic fields. Two inversion experiments are carried out: One using the inline electric field only, which we assume is the most acquired component, and one using the four horizontal electromagnetic components, which are all required to obtain the reflection response using interferometry by MDD. For the vertical conductivity of the overburden, an inversion of the full electromagnetic fields gives results similar to the joint inversion of the two reflection responses. For the horizontal conductivity of the overburden layer, the same results are achieved as for the inversion of the TE-mode reflection response only. Although for the vertical conductivity of the reservoir, an inversion of the electromagnetic fields is superior compared with an inversion of any of the reflection responses, for the horizontal conductivity of the reservoir, the in-

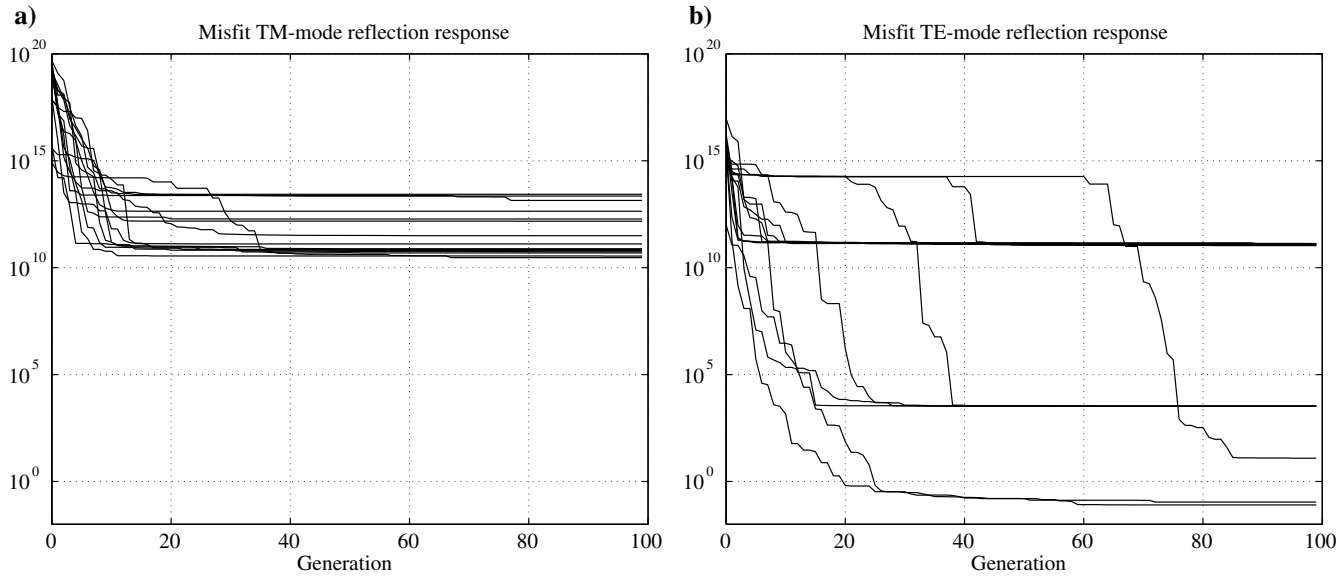

Figure 3. Convergence history of the inversion using the genetic algorithm for (a) the TM-mode and (b) the TE-mode reflection responses.

version of the TE-mode reflection response provides the best estimate.

These results show that an inversion of TE-mode reflection response is useful for finding the horizontal conductivity of the subsurface, especially of the reservoir. However, for the vertical conductivity, the full electromagnetic fields give similar or better results. Thus, inverting reflection responses can only help in getting better estimates of the horizontal conductivity. Interestingly, although the TM-mode reflection response shows a higher sensitivity to the conductivity of the reservoir than the TE-mode reflection response (Hunziker et al., 2013), the TE-mode reflection response produces better results in the inversion. We speculate that this might be because the shape of the solution space is more favorable for the TE-mode reflection response than for the TM-mode reflection response.

Conjugate-gradient algorithm

To test if the results obtained with the genetic algorithm are independent of the choice of algorithm, we invert the data also with a nonlinear conjugate-gradient algorithm. As mentioned earlier, this algorithm is included in this paper. We hope that other researchers continue to experiment with the inversion of the reflection response using their own models. For our experiments, we use the same subsurface model as for the genetic algorithm, but because our conjugate-gradient algorithm cannot handle anisotropy, we use isotropic medium parameters given in brackets in Figure 1.

We invert the TM- and TE-mode reflection responses, as well as the inline electric field separately using two different weighting functions w (equation 2). The first weighting function is one everywhere, which is in fact an inversion process without any weight.

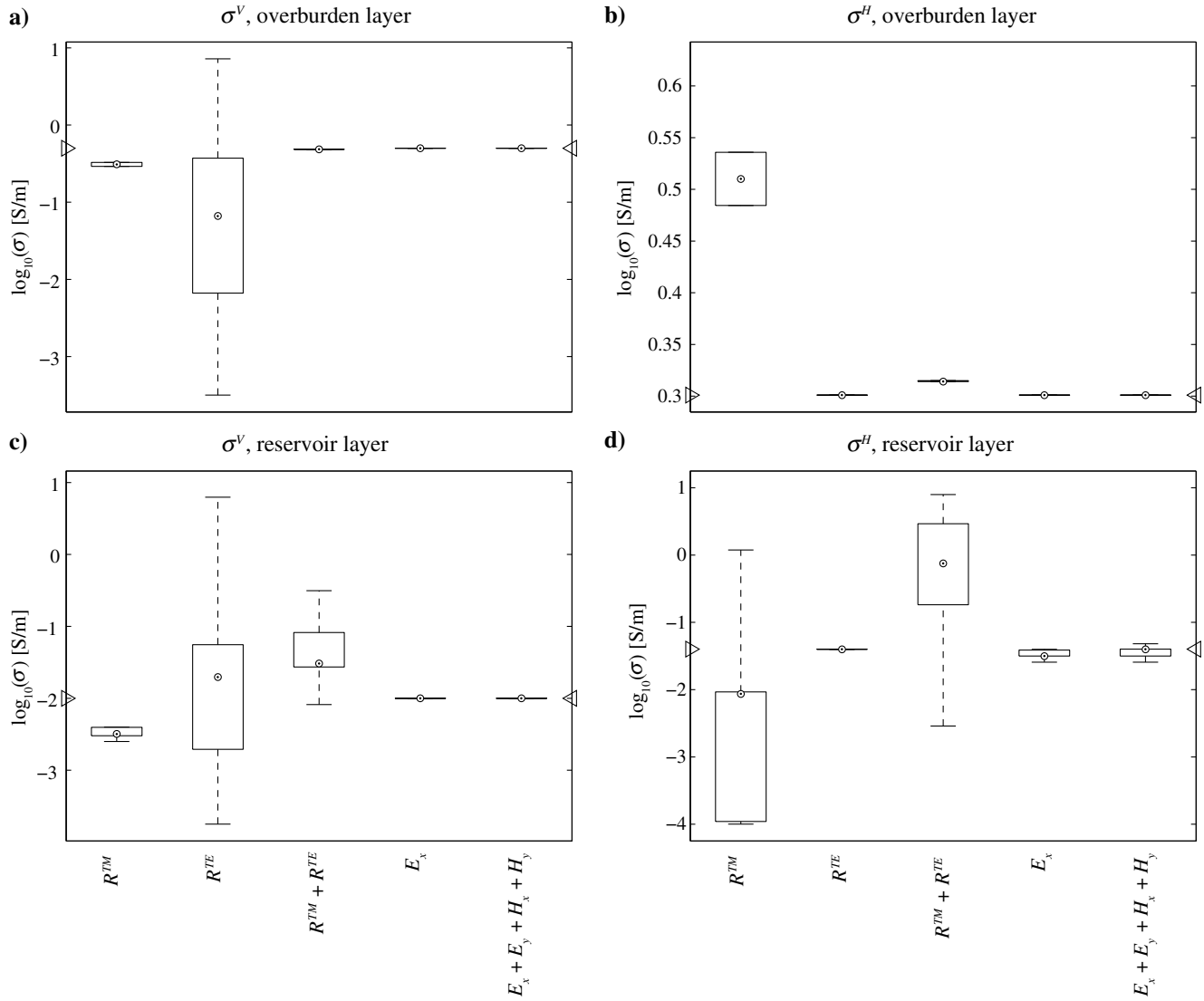

Figure 4. Boxplots for the parameter estimates of (a) vertical conductivity of the overburden layer, (b) horizontal conductivity of the overburden layer, (c) vertical conductivity of the reservoir layer, and (d) horizontal conductivity of the reservoir layer. Boxplots are shown for the following five experiments: (1) Inversion of the TM-mode reflection response only (R^{TM}), (2) TE-mode reflection response only (R^{TE}), (3) joint inversion of the TM-mode and the TE-mode reflection responses ($R^{\mathrm{TM}} + R^{\mathrm{TE}}$), (4) inversion of the inline oriented electric field (E_x), and (5) inversion of all four horizontal electromagnetic components ($E_x + E_y + H_x + H_y$). An explanation of the boxplots is given in the text. The triangle at the edges of each figure indicates the true value of the parameter.

The second weighting function is a 2D exponential function, whose exponential factors are chosen such that the data have similar amplitude at all offsets. This increases the relative importance of data at larger offsets in the misfit function. We denote this second option as "with weights."

Also for these experiments, we first have a look at the convergence history (Figure 5) before presenting the actual results. The algorithm starts with an initial guess of the subsurface parameters and optimizes this guess until the update of the model parameters is for several iterations smaller than 10^{-7}S/m or until the 500th iteration has been computed. The inversion of the TM-mode reflection response stops in our case after 12 (without weights) or 10 (with weights) iterations, whereas the inversion of the TE-mode reflection response runs until the maximum amount of 500 iterations is reached. However, for most of the later iterations, the decrease in misfit is very small. Obviously, the stopping condition chosen was too strict. Therefore, for our analysis we do not use the results of the last iteration that was computed, but the results of the last iteration that brought a relevant change of the model. The results shown below correspond to the last iteration depicted in Figure 5. Contrary to the genetic algorithm, the misfit of the TE-mode reflection response decays over fewer orders of magnitude than the misfit of the TM-mode reflection response.

The inversion results for the conjugate-gradient algorithm are shown in Figure 6. As for the genetic algorithm, we fix the conductivity of the air and the water layer (as indicated in Figure 6 with a light-gray area) and invert only for the three remaining conductivities assuming the layer thicknesses are known. As we pointed out for the genetic algorithm, this is a small and simple problem designed to find the limitations of this method. Besides that, these experiments serve as illustrative examples, but are not intended to represent a real data set. As a starting model, we use a homogeneous half-space below the receivers with a conductivity of 0.5 S/m. The inversion of the TM-mode reflection response finds the conductivity of the overburden very well, no matter if weights are applied or not. However, for the reservoir and the underburden, the solution found by the algorithm stays at the starting model. If the TE-mode reflection response is inverted, the algorithm finds the reservoir layer, but leaves the conductivity of the reservoir in the neighborhood of the conductivity of the starting model. The inversion of the inline electric field gives a result slightly inferior than the inversion of the TE-mode reflection response. As for the genetic algorithm,

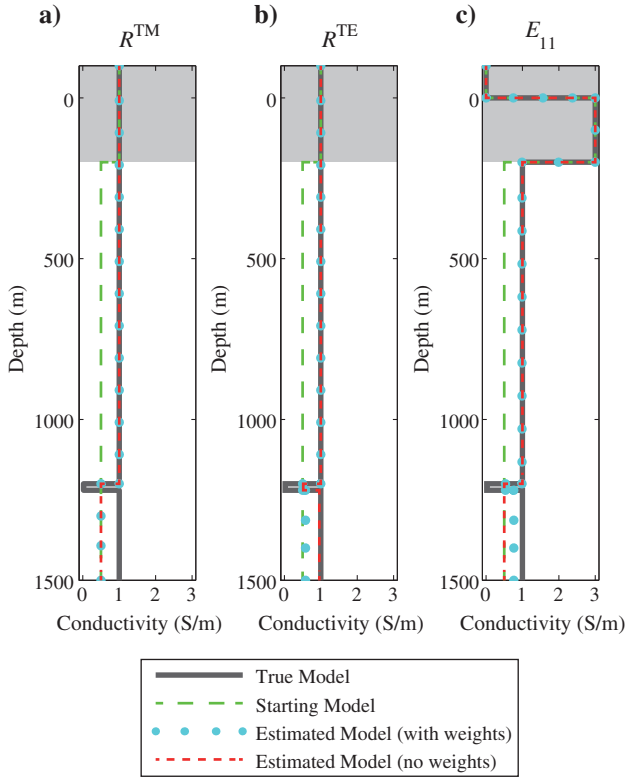

Figure 6. Inversion results for the conjugate-gradient algorithm for (a) TM-mode reflection response, (b) TE-mode reflection response, and (c) inline electric field. The true model is given in each plot as a thick dark-gray line. The starting model is drawn with a dashed green line. The inversion results without weights are depicted with a dashed red line and the inversion results with weights with blue dots. The light-gray shaded area covering the top 200 m indicates the area where the material parameters are fixed and, thus, not estimated by the inversion algorithm.

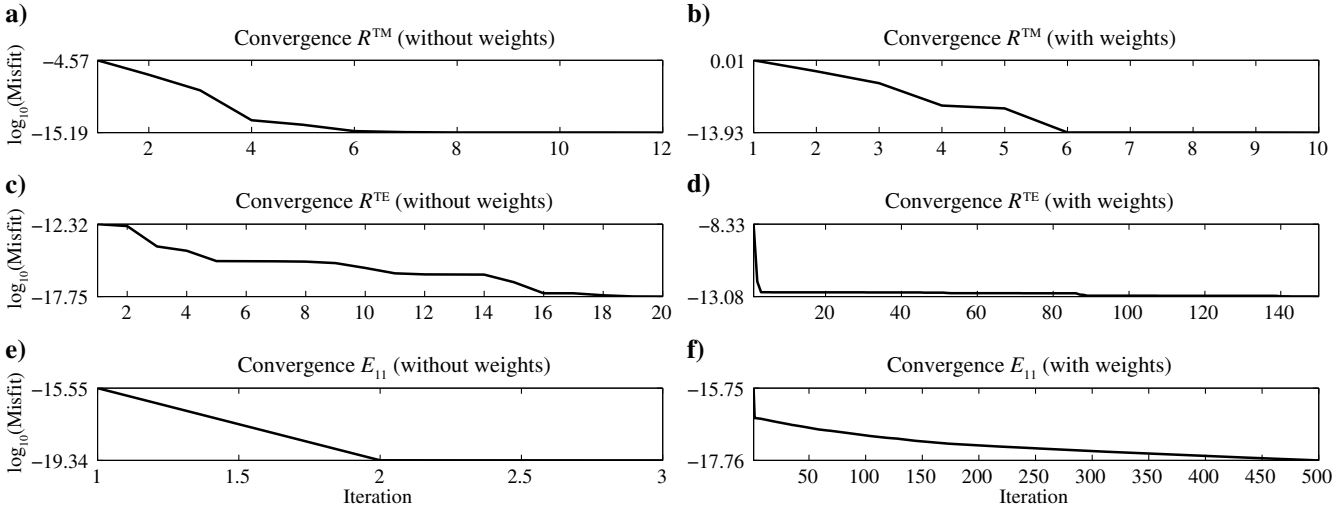

Figure 5. Convergence history of the inversion using the conjugate-gradient algorithm: TM-mode reflection response (a) without and (b) with weights, TE-mode reflection response (c) without and (d) with weights and inline electric field (e) without and (f) with weights.

the TE-mode inversion gives better results than the TM-mode inversion. This confirms our findings obtained by the inversion using the genetic algorithm.

Interestingly, the inversion of the TE-mode reflection response provides a better estimate without weights, whereas the inversion of the inline electric field provides a better estimate if weights are used. To understand the reasons for this behavior, we have to look at the data error (Figure 7), which is the relative difference between the original data and the data modeled based on the model retrieved by inversion. First, we compare the relative error for the inversion of the inline electric field without weights (Figure 7c) and with weights (Figure 7d). The scale of these two plots is identical. At intermediate and large offsets, the data error is plotted with a light gray color for the case without weights, but it becomes almost white for the case with weights indicating a lower data error. This shows that the weights help to fit the data better at intermediate and large offsets. Because these offsets feature more information about the subsurface than smaller offsets, fitting the larger offsets well improves the subsurface model. Why is that not the case for the inversion of the TE-mode reflection response?

The data error for the inversion of the TE-mode reflection response without weights is plotted in Figure 7a. Looking at the scale, we immediately see that the data error is much larger for the TE-mode reflection response than for the inline electric field. The reason is that the TE-mode reflection response decays to smaller values with offset much faster than the inline electric field. That means, by computing the relative error, we are dividing by much smaller values at large offsets blowing up even small errors to large values. This can clearly be seen in Figure 7a, where the error is relatively small for the area where the data have a large amplitude but grows very big for the large offsets, where the data have a smaller amplitude.

The reason why weights do help the inversion process for the inline electric field, but do not improve the result for the inversion of the TE-mode reflection response, lies in the structure of the two data sets. The inline electric field is at short offsets dominated by the direct field, whereas the subsurface response is only dominant at intermediate offsets. Thus, using offset-dependent weights forces the algorithm to find a better fit for the data at larger offsets. Because at those offsets the information about the subsurface is actually stored, a better subsurface model is retrieved, as we have seen above for the inline electric field. However, the reflection response is free of the direct field and free of the airwave. Therefore, the subsurface information is dominant at all offsets. Adding weights does not force the algorithm in this case to find a better subsurface model, it just alters the shape of the solution space. Such an alteration can also be for the worse. This is obviously the case in this situation. The algorithm converges less well, ending with a worse model and, thus, with a worse data error (Figure 7b).

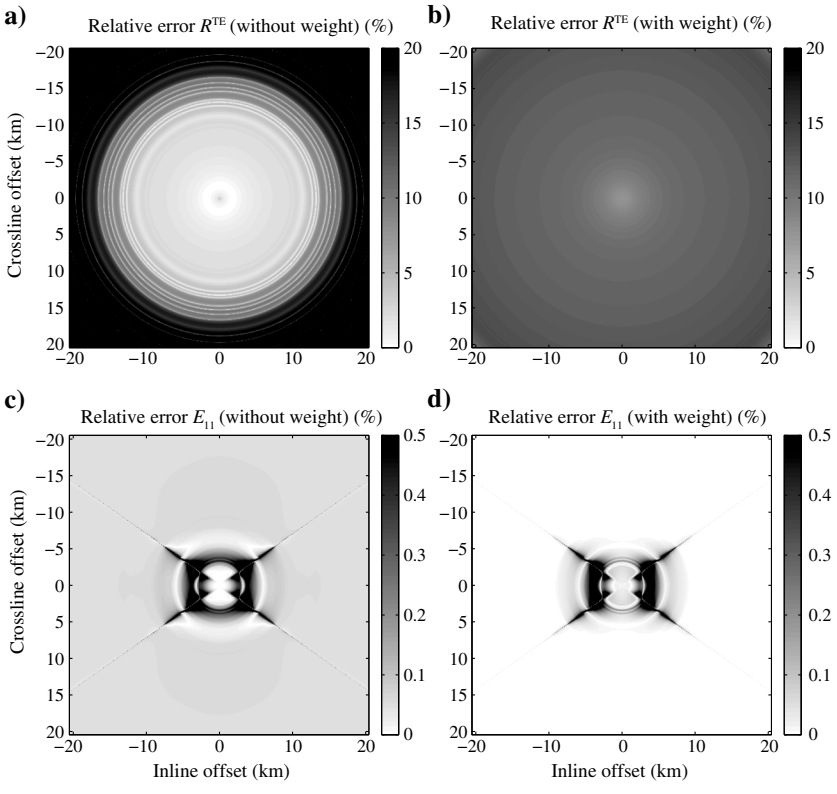

Figure 7. Relative error between the true and the modeled data based on the inversion results shown in Figure 6 for (a) TE-mode reflection response without weights, (b) TE-mode reflection response with weights, (c) inline electric field without weights, and (d) inline electric field with weights.

DISCUSSION

It is important to realize that in the experiments presented here, the source position and orientation as well as the conductivity of the water were perfectly known. If there is an error in these parameters, the reflection responses will be unaffected (Wapenaar et al., 2008) because they do not depend on these parameters at all. Thus, for strong variations in water conductivity or high-source position and orientation uncertainties, an inversion of the reflection responses might produce better results than an inversion using the full electromagnetic fields. On the other hand, retrieving the reflection responses requires the conductivity of the sediment at the ocean bottom. If there is an error in this parameter, the retrieved reflection responses will not be correct and lead to faulty estimates of the conductivity through inversion of these incorrect reflection responses.

The retrieval of the reflection responses by interferometry may also introduce artifacts if some of its assumptions are not fulfilled or the data are insufficiently sampled. For example, retrieving the reflection responses with interferometry assumes that the conductivity at the receiver level is laterally constant (Slob, 2009). In this case, an inversion of the full electromagnetic fields will lead to better estimates of the subsurface conductivities than an inversion of the reflection responses. Furthermore, if data are only available on a line, it is not possible to retrieve the reflection responses as interferometry requires grid data. We did not include experi-

ments that demonstrate these effects because, depending on how large the errors or uncertainties are chosen, either the inversion of the reflection responses or the inversion of the original electromagnetic fields will produce better results.

CONCLUSIONS

We showed that the reflection responses retrieved by interferometry can be inverted for the subsurface conductivity distribution. The TM-mode reflection response shows a much higher sensitivity to the resistive reservoir than the TE-mode reflection response. Yet, inversion of the TE-mode reflection response using either the genetic algorithm or the conjugate-gradient algorithm produces a better estimate of the subsurface including a resistive reservoir. Thus, we can conclude that an inversion of only the TM-mode reflection response is not beneficial.

The estimates of the subsurface conductivity obtained with an inversion of the reflection responses are worse compared with an inversion of the original electromagnetic fields with respect to the vertical conductivity. Thus, we determined that the vertical conductivity cannot be resolved by inverting the reflection responses. However, we were able to get a better estimate of the horizontal conductivity, especially for the reservoir, by inverting the TE-mode reflection response compared with inverting the original electromagnetic fields. This hints at the potential of inversion of reflection responses, justifying further investigations.

Thus, if the position and orientation of the source, as well as the conductivity of the water are known with high precision, the added value of inverting the reflection responses lies only in a superior estimate of the horizontal conductivity compared with an inversion of the original electromagnetic fields. Additionally, this study showed that not only the TM-mode, but also the TE-mode contains useful information for an inversion.

ACKNOWLEDGMENTS

This work is supported by the Netherlands Research Center for Integrated Solid Earth Science. We thank Cray, the supercomputing company, for allowing us to run our genetic algorithm on one of their computers for preliminary results. We thank SURFsara (www.surfsara.nl) for support in using the Cartesius Compute Cluster for computing the final results. We thank the four anonymous reviewers and the associate editor J. Dellinger for their comments.

REFERENCES

Bakulin, A., and R. Calvert, 2006, The virtual source method: Theory and case study: Geophysics, **71**, no. 4, SI139–SI150, doi: 10.1190/1.2216190.

Brown, V., K. Key, and S. Singh, 2012, Seismically regularized controlled-source electromagnetic inversion: Geophysics, **77**, no. 1, E57–E65, doi: 10.1190/geo2011-0081.1.

Christensen, N., and K. Dodds, 2007, 1D inversion and resolution analysis of marine CSEM data: Geophysics, **72**, no. 2, WA27–WA38, doi: 10.1190/1.2437092.

Constable, S., 2010, Ten years of marine CSEM for hydrocarbon exploration: Geophysics, **75**, no. 5, 75A67–75A81, doi: 10.1190/1.3483451.

Draganov, D., K. Wapenaar, and J. Thorbecke, 2006, Seismic interferometry: Reconstructing the earth's reflection response: Geophysics, **71**, no. 4, SI61–SI70, doi: 10.1190/1.2209947.

Fan, Y., R. Snieder, E. Slob, J. Hunziker, J. Singer, J. Sheiman, and M. Rosenquist, 2010, Synthetic aperture controlled source electromagnetics: Geophysical Research Letters, **37**, L13305, doi: 10.1029/2010GL043981.

Goldberg, D. E., 1989, Genetic algorithms in search, optimization, and machine learning: Addison Wesley.

Grayver, A., R. Streich, and O. Ritter, 2014, 3D inversion and resolution analysis of land-based CSEM data from the Ketzin storage formation: Geophysics, **79**, no. 2, E101–E114, doi: 10.1190/geo2013-0184.1.

Hunziker, J., E. Slob, Y. Fan, R. Snieder, and K. Wapenaar, 2012, Two-dimensional controlled-source electromagnetic interferometry by multidimensional deconvolution: Spatial sampling aspects: Geophysical Prospecting, **60**, 974–994, doi: 10.1111/j.1365-2478.2011.01019.x.

Hunziker, J., E. Slob, Y. Fan, R. Snieder, and K. Wapenaar, 2013, Electromagnetic interferometry in wavenumber and space domains in a layered earth: Geophysics, **78**, no. 3, E137–E148, doi: 10.1190/geo2011-0510.1.

Hunziker, J., J. Thorbecke, and E. Slob, 2015, The electromagnetic response in a layered VTI medium: A new look at an old problem: Geophysics, **80**, no. 1, F1–F18, doi: 10.1190/geo2013-0411.1.

Key, K., 2009, 1D inversion of multicomponent, multifrequency marine CSEM data: Methodology and synthetic studies for resolving thin resistive layers: Geophysics, **74**, no. 2, F9–F20, doi: 10.1190/1.3058434.

Plessix, R. É., and W. A. Mulder, 2008, Resistivity imaging with controlled-source electromagnetic data: Depth and data weighting: Inverse Problems, **24**, 034012–034022, doi: 10.1088/0266-5611/24/3/034012.

Ramananjaona, C., L. MacGregor, and D. Andreis, 2011, Sensitivity and inversion of marine electromagnetic data in a vertically anisotropic stratified earth: Geophysical Prospecting, **59**, 341–360, doi: 10.1111/j.1365-2478.2010.00919.x.

Ray, A., D. Alumbaugh, G. Hoversten, and K. Key, 2013, Robust and accelerated Bayesian inversion of marine controlled-source electromagnetic data using parallel tempering: Geophysics, **78**, no. 6, E271–E280, doi: 10.1190/geo2013-0128.1.

Sasaki, Y., 2013, 3D inversion of marine CSEM and MT data: An approach to shallow-water problem: Geophysics, **78**, no. 1, E59–E65, doi: 10.1190/geo2012-0094.1.

Sen, M. K., and P. L. Stoffa, 1995, Global optimization methods in geophysical inversion: Elsevier Science.

Shewchuk, J. R., 1994, An introduction to the conjugate gradient method without the agonizing pain: School of Computer Science Carnegie Mellon University Pittsburgh, http://www.cs.cmu.edu/~quake-papers/painless-conjugate-gradient.pdf, accessed 19 July 2010.

Slob, E., 2009, Interferometry by deconvolution of multicomponent multi-offset GPR data: IEEE Transactions on Geoscience and Remote Sensing, **47**, 828–838, doi: 10.1109/TGRS.2008.2005250.

Tukey, J. W., 1977, Exploratory data analysis: Addison Wesley.

Wapenaar, K., and J. Fokkema, 2006, Green's function representations for seismic interferometry: Geophysics, **71**, no. 4, SI33–SI46, doi: 10.1190/1.2213955.

Wapenaar, K., E. Slob, and R. Snieder, 2008, Seismic and electromagnetic controlled-source interferometry in dissipative media: Geophysical Prospecting, **56**, 419–434, doi: 10.1111/j.1365-2478.2007.00686.x.

Wiik, T., K. Hokstad, B. Ursin, and L. Mütschard, 2013, Joint contrast source inversion of marine magnetotelluric and controlled-source electromagnetic data: Geophysics, **78**, no. 6, E315–E327, doi: 10.1190/geo2012-0477.1.